Jurnal Penelitian Fisika dan Aplikasinya (JPFA)
Volume 16, Issue 01, 1-10 2026
https://journal.unesa.ac.id/index.php/jpfa/
p-ISSN: 2087-9946
e-ISSN: 2477-1775

Thermally Driven Phase Transformation and Structural Evolution of Hydrothermally Synthesized MoS_2

Muhammad Saukani [1,a*], Yuli Panca Asmara[1,b], Lutvi Vitria Kadarwati[2,c], and Sadang Husain [3,d]
[1] Department of Mechanical Engineering, Faculty of Engineering, Universitas Islam Kalimantan MAB, Banjarmasin 70124, Indonesia.
[2] International Ph.D. Program in Biomedical Engineering, College of Biomedical Engineering, Taipei Medical University, Taipei City 110, Taiwan
[3] Department of Physics, Faculty of Mathematics and Natural Sciences, Universitas Lambung Mangkurat, Banjarbaru, Indonesia.

e-mail: [a*] saukani@uniska-bjm.ac.id, [b] ypanca@hotmail.com, [c] d845113004@tmu.edu.tw, and [d] sadanghusain@ulm.ac.id
* Corresponding Author

Received: 8 Febuary 2026; Revised: 21 May 2026; Accepted: 24 June 2026

Abstract

Molybdenum disulfide (MoS_2) is a transition-metal dichalcogenide with tunable physicochemical properties that strongly depend on its crystal phase. Although the phase transformation from 1T to 2H-MoS_2 has been extensively discussed, the early-stage thermal transition behavior of hydrothermally synthesized MoS_2 remains insufficiently understood. In this work, MoS_2 was synthesized via hydrothermal synthesis and then annealed at 200°C and 300°C to investigate its thermally induced phase transformation. The structural evolution was investigated by X-ray diffraction (XRD) and Raman spectroscopy, and the morphology was examined by SEM and TEM. Raman spectra of the sample before annealing showed characteristic 1T-MoS_2 peaks at around 146, 229, and 331 cm^{-1}, corresponding to the J1, J2, and J3 vibrational modes. After annealing at 300°C, these peaks disappeared and were replaced by the E_{2g} and A_{1g} modes at approximately 375 and 403 cm^{-1}, indicating the formation of the thermodynamically stable 2H phase. XRD analysis further confirmed the phase transformation by shifting the dominant (002) peak from $2\theta \approx 9.3°$ to 14.4°. In addition, the crystallinity increased from 67.48% in the pre-annealing sample to 72.64% and 75.66% after annealing at 200°C and 300°C, respectively. The crystallite size also increased from 30.01 nm to 39.51 nm and 39.89 nm following thermal treatment. Despite these structural changes, SEM and TEM observations revealed that the flower-like morphology was largely preserved after annealing. Overall, these results provide a clearer understanding of the phase evolution in hydrothermally synthesized MoS_2 and exhibit how thermal treatment can be used to tune its properties. Such phase-dependent characteristics make MoS_2 a promising material for photothermal, sensing, energy-storage, electronic, and optoelectronic applications.

Keywords: *phase transformation; 1T-MoS_2; 2H-MoS_2; hydrothermal synthesis.*

How to cite: Saukani M, Asmara YP, Husain S. Thermally Driven Phase Transformation and Structural Evolution of Hydrothermally Synthesized MoS_2. *Jurnal Penelitian Fisika dan Aplikasinya (JPFA)*. 2026; 16(1): 1-10. DOI: https://doi.org/10.26740/jpfa.v16n1.p1-10.

DOI: 10.26740/jpfa.v16n1.p1-10

INTRODUCTION

Molybdenum disulfide (MoS_2) is a transition-metal dichalcogenide with a unique layered structure and tunable physicochemical properties. This material enables versatile phase and morphology engineering via both top-down and bottom-up synthesis. It has been reported to form various nanostructures, such as nanosheets and nanoflowers, with high surface area and tunable electronic properties [1]. Therefore, enabling broad applications in energy conversion and storage [2–5], electronics [5–8], environmental [9–11], and medical [12–16] applications.

The properties of MoS_2 strongly depend on its crystal phase. In bulk form, MoS_2 naturally exists in the thermodynamically stable 2H phase with trigonal prismatic coordination, and exhibits semiconducting behavior with an indirect bandgap of ~1.29 eV, while monolayer 2H-MoS_2 possesses a direct bandgap of 1.9 eV, making it promising for electronic and optoelectronic applications [2,3]. In comparison, the metastable 1T phase exhibits metallic conductivity and has been widely reported to deliver superior performance in electrochemical applications, including electrocatalysis and energy storage. However, despite these advantages, the 1T phase is thermodynamically metastable and tends to revert into the thermodynamically stable 2H phase under external stimuli, particularly thermal treatment [4]. Therefore, the phase transformation between 1T and 2H has been intensively investigated because it directly modifies the electronic structure and governs the functional performance of MoS_2. [3,5].

Generally, the 1T phase is obtained through top-down approaches, such as plasma exfoliation and lithium intercalation [3,6]. The phase transformation upon annealing has been extensively studied. The lithium intercalation process causes electron transfer to the MoS_2 layers, which induces a change in the coordination of molybdenum atoms from trigonal prismatic to octahedral, thereby imparting a metallic 1T structure [7]. Nevertheless, the 1T phase produced by this method is metastable and susceptible to relaxation back to the 2H phase upon removal of the intercalator or upon thermal treatment, such as annealing in an inert atmosphere at temperatures around 200 °C [4,8,9].

In addition to the top-down approach, bottom-up methods such as chemical vapor deposition (CVD) and hydrothermal have also been widely used for the synthesis of MoS_2 [10–12]. The CVD method can produce MoS_2 with high crystallinity but generally requires a high growth temperature of 780–800 °C [13]. In contrast, the hydrothermal method offers a simpler, more energy-efficient synthesis route and does not involve ionic intercalators. Mutalik et al. reported that the 1T-MoS_2 phase can be produced by the hydrothermal method, and that the phase transformation to the 2H structure can be achieved by annealing at relatively low temperatures, such as 300 °C [6].

Although the 1T-2H phase has been widely discussed, systematic investigations of the thermal transition window in hydrothermally synthesized MoS_2 remain limited, particularly compared with the lithium intercalation method. Previous studies have primarily focused on annealing temperatures in the range of 400–800 °C, where enhanced crystallization and improved structural properties of 2H-MoS_2 were reported [14]. However, the early-stage phase transition behavior at lower temperatures remains insufficiently understood. Therefore, the purpose of this study is to identify the critical temperature range governing the phase transformation of hydrothermally synthesized MoS_2 by examining its structural evolution at selected annealing temperatures. Annealing temperatures of 200 °C and 300 °C were chosen to represent the transitional and fully transformed states based on a prior study [4,6,15]. X-ray diffraction (XRD) was used to identify crystallographic evolution, while Raman spectroscopy was used to confirm phase characteristics.

Scanning electron microscopy (SEM) and transmission electron microscopy (TEM) were used to evaluate morphological stability during the phase transformation process.

METHOD

Synthesis of MoS_2

MoS_2 was synthesized via the hydrothermal method. Briefly, 0.032 g of molybdic acid (H_2MoO_4, Acros Organic) as a source of molybdenum and 0.038 g of thiourea ($SC(NH_2)_2$, Acros Organic) as a source of sulfur were dissolved in 40 mL of deionized (DI) water under magnetic stirring at 500 rpm for 40 minutes at room temperature until the initial milky white suspension became transparent. The homogenous solution was then transferred into a Teflon-lined stainless-steel autoclave and heated at 180°C for 24 hours. After naturally cooling to room temperature, the precipitate was collected by centrifugation at 7500 rpm, washed twice with DI water, and then with ethanol. The product was dried at 65°C for 24 hours. To investigate the phase transformation, the dried MoS_2 product was annealed in a tubular furnace under an N_2 atmosphere at 200°C and 300°C for 2 hours.

Material Characterization

The structural and morphological properties of the MoS_2 hydrothermal product and annealed MoS_2 samples were characterized using Raman spectroscopy, XRD, SEM, and TEM. Raman measurements were conducted using a micro-Raman mapping system (UniDron, Uninanotech) with a 632 nm laser to identify phase evolution in samples before and after annealing at 300 °C. The crystal structure was analyzed by XRD (D2 Phaser, Bruker) using Cu Kα radiation, performed on samples before and after annealing at 200 °C and 300 °C. Phase identification was carried out using the PDF-2 database in X'Pert HighScore Plus software. The morphology of the samples before and after annealing at 300 °C was observed using SEM (SU3500, Hitachi) at 15 kV and TEM (HT7700, Hitachi) at 75 kV.

RESULTS AND DISCUSSION

Phase Transformation Analysis of MoS_2

The phase transformation of MoS_2 was investigated by Raman spectroscopy. The Raman spectra for hydrothermally synthesized MoS_2 before and after annealing are shown in Figure 1. Generally, 1T-MoS_2 is characterized by several low-frequency Raman phonon peaks, namely J_1 (~150 cm^{-1}), J_2 (~225 cm^{-1}), and J_3 (~330 cm^{-1}), which are associated with metallic phase behavior. In contrast, monolayer 2H-MoS_2 typically exhibits two Raman mode, E_{2g} and A_{1g}, located at the Raman shift ~403 cm^{-1} and ~384 cm^{-1}, respectively [4,13,16,17].

The Raman spectra of hydrothermally synthesized MoS_2 before annealing in Figure 1(black line), displays several peaks, namely at ~146 cm^{-1}, ~229 cm^{-1}, and ~331 cm^{-1}, corresponding J_1, J_2, and J_3, respectively. In addition, peaks observed at ~277 cm^{-1} and ~370 cm^{-1} were assigned to E_{1g} and E_{2g} vibrational modes, respectively. Although slight shifts from previously reported values were observed, these shifts are commonly attributed to the structurally distorted nature of metastable 1T-MoS_2 and to local disorder in chemically synthesized samples. The J_1 mode is associated with out-of-plane vibrations and in-plane shearing motions of Mo atoms within the zigzag chain structure. Meanwhile, the J_2 mode corresponds to the relative displacement of sulfur atomic layers relative to the Mo atoms. The J_3 peak originates from vibrational splitting of the zigzag

Mo chains, accompanied by a slight out-of-plane component [18].

After annealing at 300 C, the $J_1 - J_3$ peaks disappear, while two dominant peaks emerged at Raman Shift 375 cm^{-1} and 403 cm^{-1}, which correspond to E_{2g} and A_{1g} vibrational modes of the 2H-MoS_2 phase, respectively [17,19–21]. The disappearance of the low-frequency J peaks indicates that, in this study, the E_{2g} peak appeared at ~375 cm^{-1} after annealing. A similar Raman shift has also been reported for hydrothermally synthesized and annealed 2H-MoS_2 nanostructures [6,15], suggesting that the vibrational characteristics of chemically synthesized MoS_2 may differ from those of mechanically exfoliated monolayer MoS_2 due to differences in structural ordering, multilayer stacking, and local atomic environments. Overall, these Raman analysis results confirmed that the annealing treatment successfully induced a phase transformation from the metastable 1T-MoS_2 to the thermodynamically stable 2H-MoS_2 phase.

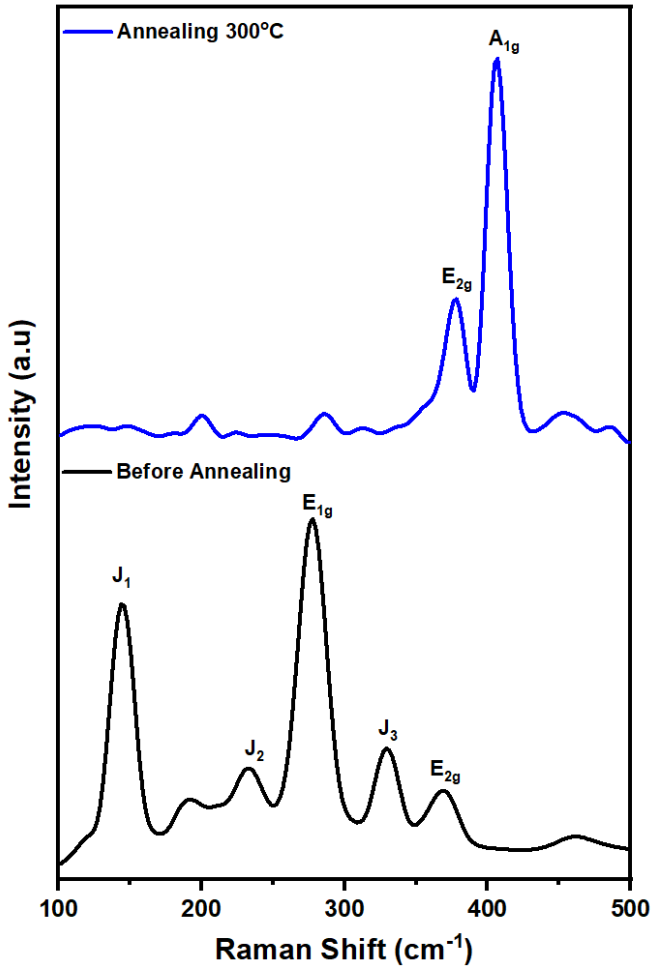

Figure 1. Raman Spectra of the hydrothermally synthesized MoS_2 before annealing (black line) and after annealing at 300 °C (blue line).

Crystal Structure Analysis

The XRD patterns of MoS_2 before and after annealing at 200°C and 300°C are shown in Figure 2(a). Increasing the annealing temperature alters the diffraction pattern, indicating changes in the crystal structure. Before annealing, the XRD pattern exhibited diffraction peaks corresponding to the (002), (004), (100), and (110) with 2θ values of approximately 9.3°, 17.8°, 32.9°, and 58°,

respectively. The (002) plane at 2θ 9.3° shows the highest intensity, whereas the remaining were relatively broad and of low intensity. Furthermore, the relatively high background of diffraction indicates low crystallinity and poor interlayer order. These characteristics are common in metastable MoS_2, corresponding to the metallic phase of MoS_2 [6,7,22,23]. The present synthesis route also produces better crystallinity (67.48%) than the hydrothermal method reported by Chen et al., which employe ammonium heptamolybdate tetrahydrate as a Molybdenum source and thioacetamide as a sulfur source for the hydrothermal route, yielding MoS_2 with an impurity phase and low crystallinity [9].

After annealing at 200°C, the (002) plane remained observable with slightly increased intensity, whereas the other diffraction peaks remained relatively weak and poorly defined. This indicates that the structural transformation has not yet fully occurred, and the 1T-MoS_2 and 2H-MoS_2 structures may still coexist. In the sample annealed at 300°C, the XRD pattern shows exhibited more significant changes. The (002) plane becomes sharper and more intense, accompanied by a shift to 2θ of 14.4°. Qualitative analysis using X'Pert Highscore Plus indicated that the diffraction pattern (blue line in Figure 2(a)) matched the single-phase 2H-MoS_2 (JCPDS 37-1492) [24]. These results indicate that annealing at 300°C effectively stabilizes the trigonal prismatic MoS_2 structure. This trend aligns with the Raman analysis results, which demonstrated a phase transformation from metastable MoS_2 to the thermodynamically stable 2H phase, although the annealing temperature used in this study was is lower than that reported by Pham et al. [25].

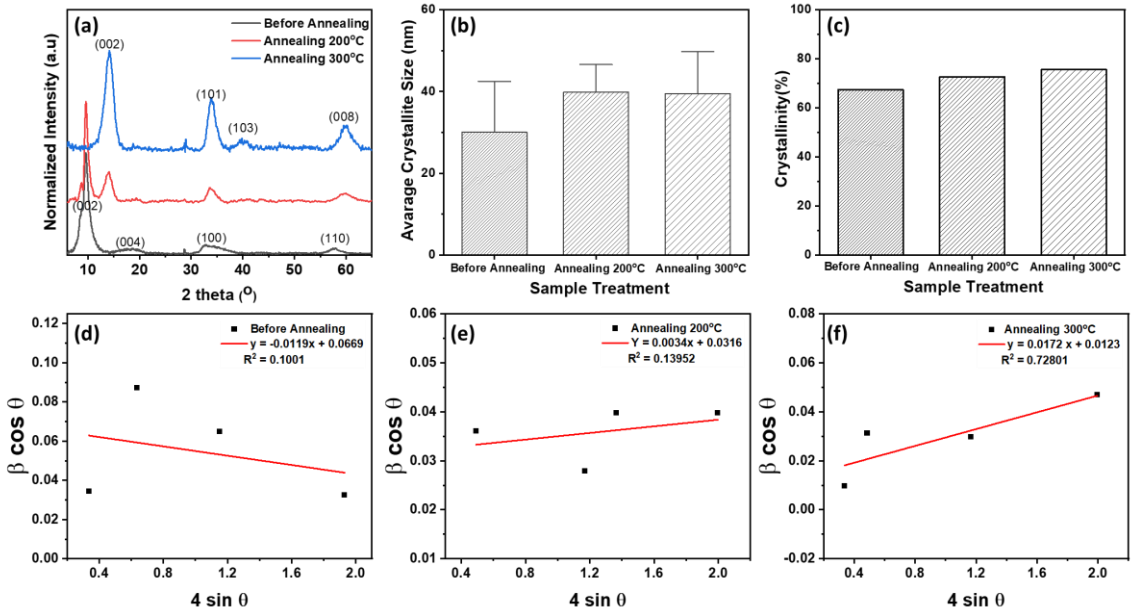

Figure 2. (a) The XRD patterns of hydrothermally synthesized MoS_2 (black line), after annealing at 200°C (red line), and after annealing 300°C (blue line), (b) the average crystallite size of hydrothermally synthesized MoS_2 with different sample treatment, (c) the crystallinity of hydrothermally synthesized MoS_2 with different sample treatment, (d) plot graph between 4 sin θ vs β cos θ for hydrothermally synthesized MoS_2 before annealing, (e) plot graph between 4 sin θ vs β cos θ for hydrothermally synthesized MoS_2 after annealing 200 °C, (f) plot graph between 4 sin θ vs β cos θ for hydrothermally synthesized MoS_2 after annealing 300 °C.

Furthermore, the crystallite size of the samples subjected to different thermal treatments was calculated using the Scherrer equation [26]:

$$D = \frac{K\,\lambda}{\beta \cos\theta} \quad (1)$$

where D is the crystallite size, K is the Scherrer constant (0.9), λ is the wavelength of Cu-Kα radiation (1.54184 nm), θ is the Bragg diffraction angle, and β is the full width at half maximum (FWHM) value of diffraction peak. The average crystallite sizes are presented in Figure 2(b). According to the calculation, the crystallite size increased with increasing annealing temperature, namely 30.01 nm, 39.51 nm, and 39.89 nm for the samples before annealing, annealing at 200 °C, and annealing at 300 °C, respectively. Similarly, thermal treatment also increased the crystallinity of the samples from 67.48% for before annealing to 72.64% and 75.66% after annealing at 200°C and 300°C, respectively, as shown in Figure 2(c). The gradual increase in crystallinity indicates improved structural ordering and stabilization of the thermodynamically stable 2H-MoS_2 phase with increasing annealing temperature.

Thermal treatment affected the lattice strain of the crystal structure. The Williamson–Hall equation was employed to evaluate the lattice strain (η) using equation (2):

$$\beta \cos\theta = \frac{K\,\lambda}{D} + 4\eta \sin\theta \quad (2)$$

The lattice strain was determined from the slope of the Williamson-Hall plot between 4 sin θ in the x-axis and cos θ in the y-axis, as shown in Figure 2(d) – (f). The hydrothermally synthesized MoS_2 before annealing exhibited a negative lattice strain value of -0.0119, indicating compressive strain associated with the distorted metastable 1T structure and a high defect density. After annealing, the slope becomes positive, with strain values of 0.0034 and 0.0172 for the samples annealed at 200 C and 300 C, respectively. This behavior suggests lattice rearrangement and strain evolution toward a more ordered 2H structure. This observation is consistent with the Raman results, which showed the disappearance of the J peaks and the emergence of dominant 2H vibrational modes, confirming the phase transformation and improved crystallinity of the MoS_2 samples.

In addition to thermal energy, several structural factors may also influence the phase transformation behavior of MoS_2. The metastable 1T phase generally contains a higher defect density and lattice distortion than the stable 2H structure, which contributes to the negative strain observed before annealing. Thermal treatment gradually reduces these distortions and promotes structural relaxation toward a more ordered crystal structure. Residual species originating from hydrothermal precursors may also affect the stability of the metastable phase by modifying the local atomic environment during synthesis [8]. Compared with lithium-intercalated MoS_2 systems, the hydrothermally synthesized MoS_2 in this study required a relatively higher temperature to achieve complete transformation into the 2H phase. In lithium-intercalated MoS_2, electron transfer from intercalated Li atoms weakens interlayer interactions and facilitates structural rearrangement, allowing phase transformation to occur at lower temperatures [4]. In contrast, the hydrothermal route used in this work does not involve intercalating species, resulting in a different stabilization mechanism and thermal transition behavior [6,25].

Morphology Analysis

Previous characterization using Raman spectroscopy or XRD indicated that both samples exhibit phase differences, confirming the transition from 1T-MoS_2 (metallic) to 2H-MoS_2 (semiconductor). The morphologies of the samples before and after annealing treatment are shown

in Figure 3. Although the previous data show different phases, the SEM images in Figures 3(a) and (b) show similar morphology, a flower-like structure. The surface morphology does not change significantly, indicating that the material phase does not significantly affect the basic shape of the surface structure, even after annealing up to 350°C [25]. Furthermore, deep morphological analysis was performed using TEM, as shown in Figures 3(c) and 3(d). Both morphology samples also show similar morphologies. Therefore, this result indicates that, despite the effect of annealing on phase transformation at the crystalline level from octahedral to trigonal prismatic, the surface morphology and internal structure of the two phases remain significantly similar, with no discernible differences at the TEM resolution used.

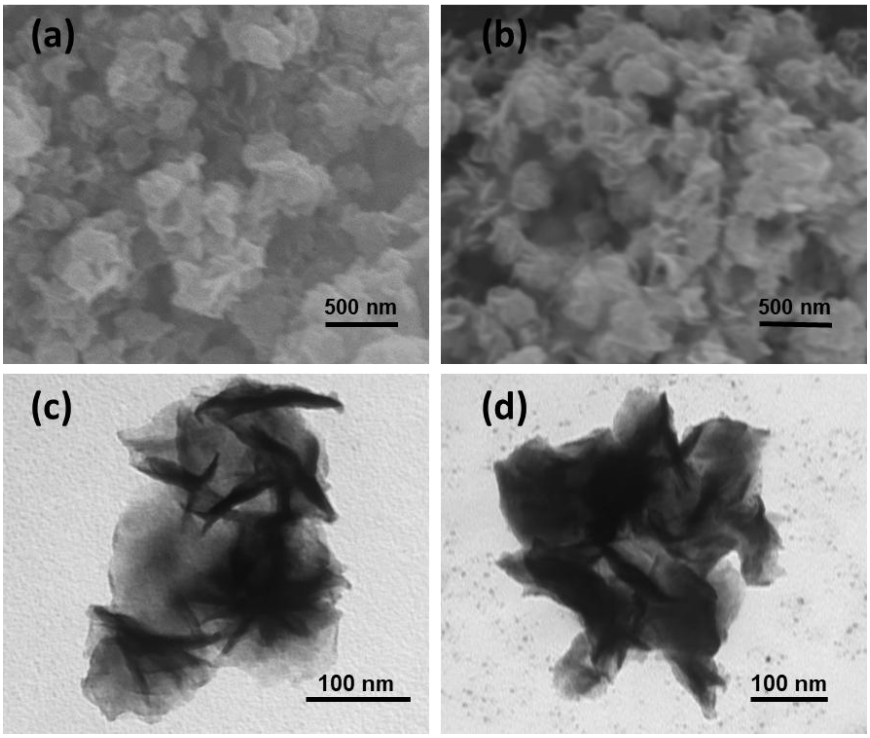

Figure 3. Morphological characterization of MoS_2, (a) SEM image of 1T-MoS_2, (b) SEM image of 2H-MoS_2, (c) TEM image of 1T-MoS_2, and (d) TEM image of 2H-MoS_2.

Although Raman spectroscopy and XRD confirm a clear phase transformation from metallic 1T-MoS_2 to semiconducting 2H-MoS_2 after annealing treatment, SEM and TEM analyses reveal that the overall flower-like morphology remains unchanged. Importantly, several previous studies reporting phase transformation at relatively low temperatures (~200 °C) are based on lithium-intercalated bulk MoS_2, in which the 1T phase is induced by charge transfer and lattice expansion [4,8,9]. In contrast, the hydrothermal, intercalator-free synthesis in this study yielded a metastable 1T phase that required annealing at 300 °C to fully stabilize to the 2H phase. These findings demonstrate that the phase stability of MoS_2 strongly depends on the synthesis route and highlight the potential of hydrothermally synthesized MoS_2 for applications that require structural integrity and thermal robustness.

CONCLUSION

MoS_2 was successfully synthesized using the hydrothermal method and showed significant structural changes after annealing. Raman analysis confirmed that MoS_2 before annealing was dominated by the metastable 1T phase, characterized by the appearance of J_1–J_3 peaks as phonon modes at approximately 146, 229, and 331 cm^{-1}. After annealing at 300°C led to the disappearance of phonon modes and the emergence of the E_{2g} and A_{1g} modes at around 375 and 403 cm^{-1}, indicating transformation into the thermodynamically stable 2H-MoS_2 phase. XRD results showed an increase in crystallinity 67.48% to 72.64% and 75.66% after annealing at 200°C and 300°C, respectively. The crystallite size increased from 30.01 nm to 39.89 nm after thermal treatment, while the lattice strain changed from −0.0119 before annealing to 0.0034 and 0.0172 after annealing at 200°C and 300°C, respectively, indicating improved structural ordering toward the stable 2H phase. Although the structural transformation was confirmed, SEM and TEM observations revealed that the flower-like morphology was retained after annealing. These findings demonstrate that thermal annealing is an effective approach for controlling the phase structure of MoS_2 while preserving its morphology. The metallic 1T phase is attractive for photothermal, electrochemical sensing, electrocatalytic, and energy-storage applications, whereas the semiconducting 2H phase is more suitable for electronic, optoelectronic, and biomedical sensing devices.

ACKNOWLEDGMENT

This Research was founded by the Universitas Islam Kalimantan Muhammad Arsyad Al Banjari through the competitive scheme with contract number: 73/UNISKA-PUSLIT/IV/2025.

AUTHOR CONTRIBUTIONS

Muhammad Saukani: Conceptualization, Methodology, Writing-original draft and Validation; Yuli Panca Asmara: Formal Analysis, Resources, and Visualization; Lutvi Vitria Kandarwati: Investigation, Software, and Project Administration; and Sadang Husain: Data Curation, Software, and Writing - Original Draft.

REFERENCES

1. Singh, A.; Baji, D.S.; Nair, S.; Santhanagopalan, D. MoS2 for Battery and Supercapacitor Applications. In *Science and Technology of 2D MoS2*; Late, D.J., Rout, C.S., Eds.; Springer Nature: Singapore, 2024; pp. 205–229 ISBN 978-981-97-7367-1.
2. Chen, Y.; Pham, T.; Mulchandani, A. 2D MoS2-Based Flexible Optoelectronic for Biosensing. *Sensors and Actuators B: Chemical* **2025**, *439*, 137848, doi:10.1016/j.snb.2025.137848.
3. Wang, Z.; Mi, B. Environmental Applications of 2D Molybdenum Disulfide (MoS2) Nanosheets. *Environ. Sci. Technol.* **2017**, *51*, 8229–8244, doi:10.1021/acs.est.7b01466.
4. Eda, G.; Yamaguchi, H.; Voiry, D.; Fujita, T.; Chen, M.; Chhowalla, M. Photoluminescence from Chemically Exfoliated MoS2. *Nano Lett.* **2011**, *11*, 5111–5116, doi:10.1021/nl201874w.
5. Kumar, P.C.; Jeong, S.M.; Naik, R.; Rout, C.S. Rhombohedral 3R MoS2 Polytype: A Promising Fundamental Material for Next-Generation Device Applications. *Small* **2025**, *21*, 2504644, doi:10.1002/smll.202504644.
6. Mutalik, C.; Krisnawati, D.I.; Patil, S.B.; Khafid, M.; Atmojo, D.S.; Santoso, P.; Lu, S.-C.; Wang, D.-Y.; Kuo, T.-R. Phase-Dependent MoS2 Nanoflowers for Light-Driven Antibacterial Application. *ACS Sustainable Chem. Eng.* **2021**, *9*, 7904–7912, doi:10.1021/acssuschemeng.1c01868.
7. Lei, Z.; Zhan, J.; Tang, L.; Zhang, Y.; Wang, Y. Recent Development of Metallic (1T) Phase of

Molybdenum Disulfide for Energy Conversion and Storage. *Advanced Energy Materials* **2018**, *8*, 1703482, doi:10.1002/aenm.201703482.

8. Zhang, M.; Wang, K.; Zeng, S.; Xu, Y.; Nie, W.; Chen, P.; Zhou, Y. Visible Light-Induced Antibacterial Effect of MoS2: Effect of the Synthesis Methods. *Chemical Engineering Journal* **2021**, *411*, 128517, doi:10.1016/j.cej.2021.128517.
9. Chen, H.; He, X.; Zhou, Z.; Wu, Z.; Li, H.; Peng, X.; Zhou, Y.; Tan, C.; Shen, J. Metallic Phase Enabling MoS2 Nanosheets as an Efficient Sonosensitizer for Photothermal-Enhanced Sonodynamic Antibacterial Therapy. *J Nanobiotechnol* **2022**, *20*, 136, doi:10.1186/s12951-022-01344-6.
10. Devendar, L.; Yadav, V.; Pothal, B.; Ganapathi, K.L.; Jaiswal, M. CVD Growth of Large-Area, Continuous, and Defect-Free MoS2 Multilayer Films from Solution-Cast Seed Nanoflakes. *Surfaces and Interfaces* **2024**, *50*, 104470, doi:10.1016/j.surfin.2024.104470.
11. Cho, Y.J.; Sim, Y.; Lee, J.-H.; Hoang, N.T.; Seong, M.-J. Size and Shape Control of CVD-Grown Monolayer MoS2. *Current Applied Physics* **2023**, *45*, 99–104, doi:10.1016/j.cap.2022.11.008.
12. Gao, Y.; Lu, S.; Hou, X.; Wang, B.; Jiang, Z.; Wang, Y.; Fang, T. Scalable Bottom-Up Synthesis of High-Purity 1T-MoS2 Assisted by Na2SO4 Template. *Small* **2025**, *21*, 2500529, doi:10.1002/smll.202500529.
13. Guo, Y.; Fu, X.; Peng, Z. Growth and Mechanism of MoS2 Nanoflowers with Ultrathin Nanosheets. *Journal of Nanomaterials* **2017**, *2017*, 6865282, doi:10.1155/2017/6865282.
14. Lamouchi, A.; Assaker, I.B.; Chtourou, R. Effect of Annealing Temperature on the Structural, Optical, and Electrical Properties of MoS2 Electrodeposited onto Stainless Steel Mesh. *J Mater Sci* **2017**, *52*, 4635–4646, doi:10.1007/s10853-016-0707-9.
15. Mutalik, C.; Okoro, G.; Chou, H.-L.; Lin, I.-H.; Yougbaré, S.; Chang, C.-C.; Kuo, T.-R. Phase-Dependent 1T/2H-MoS2 Nanosheets for Effective Photothermal Killing of Bacteria. *ACS Sustainable Chem. Eng.* **2022**, *10*, 8949–8957, doi:10.1021/acssuschemeng.2c02457.
16. Tumino, F.; D'Agosta, P.; Russo, V.; Li Bassi, A.; Casari, C.S. Raman Spectroscopy of 2D MoS2 Interacting with Metals. *Crystals* **2023**, *13*, 1271, doi:10.3390/cryst13081271.
17. Jiménez Sandoval, S.; Yang, D.; Frindt, R.F.; Irwin, J.C. Raman Study and Lattice Dynamics of Single Molecular Layers of MoS2. *Phys. Rev. B* **1991**, *44*, 3955–3962, doi:10.1103/PhysRevB.44.3955.
18. Yu, Y.; Nam, G.-H.; He, Q.; Wu, X.-J.; Zhang, K.; Yang, Z.; Chen, J.; Ma, Q.; Zhao, M.; Liu, Z.; et al. High Phase-Purity 1T′-MoS2- and 1T′-MoSe2-Layered Crystals. *Nature Chem* **2018**, *10*, 638–643, doi:10.1038/s41557-018-0035-6.
19. Thayil, R.; Parne, S.R.; Ramana, C. v. 2D MoS2 for Next-Generation Electronics and Optoelectronics: From Material Properties to Manufacturing Challenges and Future Prospects. *Small* **2025**, *21*, 2412467, doi:10.1002/smll.202412467.
20. Li, H.; Zhang, Q.; Yap, C.C.R.; Tay, B.K.; Edwin, T.H.T.; Olivier, A.; Baillargeat, D. From Bulk to Monolayer MoS2: Evolution of Raman Scattering. *Advanced Functional Materials* **2012**, *22*, 1385–1390, doi:10.1002/adfm.201102111.
21. Chakraborty, B.; Matte, H.S.S.R.; Sood, A.K.; Rao, C.N.R. Layer-Dependent Resonant Raman Scattering of a Few Layer MoS2. *Journal of Raman Spectroscopy* **2013**, *44*, 92–96, doi:10.1002/jrs.4147.
22. Zang, L.; Wang, M.; Han, Q.; Wang, Z. Phase-Dependent Properties and Applications of MoS2 in Environmental Remediation: Synthesis, Characterization, and Performance Optimization.

ACS EST Water **2024**, *4*, 4690–4707, doi:10.1021/acsestwater.4c00501.

23. Yao, Y.; Ao, K.; Lv, P.; Wei, Q. MoS2 Coexisting in 1T and 2H Phases Synthesized by Common Hydrothermal Method for Hydrogen Evolution Reaction. *Nanomaterials* **2019**, *9*, 844, doi:10.3390/nano9060844.
24. Chang, C.-J.; Tsai, Z.-T.; Lin, K.-S.; Nian, Y.-H. Enhanced Photocatalytic H2 Production of Flower-like MoS2@Ag2S Photocatalysts with Matched Band Structures. *Journal of Photochemistry and Photobiology A: Chemistry* **2023**, *445*, 115027, doi:10.1016/j.jphotochem.2023.115027.
25. Pham, M.T.; Nguyen, H.H.; Ly, Q.M.; Van Lai, D.; Lai, H.T.; Dao, T.N.; La, D.D.; Nguyen, P.M.; Thi, H.P.N. MoS2 Flower-like Architecture with Enhanced Photocatalytic Performance for Degradation of Organic Dyes under Sunlight Simulation. *Res Chem Intermed* **2025**, *51*, 7263–7281, doi:10.1007/s11164-025-05772-5.
26. Nurrohman, DT, & Pribadi, JS (2018). Study of crystal structure, lattice strain, and chemical composition of iron sand nanoparticles synthesized by ball milling method. Konstan-Jurnal Fisika dan Pendidikan Fisika , 3 (2), 94-101..